MDPI

Chemical Constituents of the Mushroom *Dictyophora indusiata* and Their Anti-Inflammatory Activities

Yingfang Zhang [1,†], Hang Xun [1,†], Quan Gao [2], Feifei Qi [3], Jia Sun [1,4,*] and Feng Tang [1,*]

[1] Key Laboratory of National Forestry and Grassland Administration Beijing for Bamboo & Rattan Science and Technology, International Centre for Bamboo and Rattan, Beijing 100102, China; zhangyingfang@ipe.ac.cn (Y.Z.); xunhang@icbr.ac.cn (H.X.)

[2] Anhui Key Laboratory of Agricultural Products, School of Resource and Environment, Anhui Agricultural University, Hefei 230036, China; 15155139755@163.com

[3] Shandong Provincial Key Laboratory of Synthetic Biology, Qingdao Institute of Bioenergy and Bioprocess Technology, Chinese Academy of Sciences, Qingdao 266101, China; qiff@qibebt.ac.cn

[4] Eurofins Agroscience Services, Hercules, CA 94547, USA

* Correspondence: lzjx2003@gmail.com (J.S.); fengtang@icbr.ac.cn (F.T.)

† These authors contributed equally to this work.

Abstract: As an edible and medicinal fungus, *Dictyophora indusiata* is well-known for its morphological elegance, distinctive taste, high nutritional value, and therapeutic properties. In this study, eighteen compounds (**1–18**) were isolated and identified from the ethanolic extract of *D. indusiata*; four (**1–4**) were previously undescribed. Their molecular structures and absolute configurations were determined via a comprehensive analysis of spectroscopic data (1D/2D NMR, HRESIMS, ECD, and XRD). Seven isolated compounds were examined for their anti-inflammatory activities using an in vitro model of lipopolysaccharide (LPS)-simulated BV-2 microglial cells. Compound **3** displayed the strongest inhibitory effect on tumor necrosis factor-α (TNF-α) expression, with an IC_{50} value of 11.9 μM. Compound **16** exhibited the highest inhibitory activity on interleukin-6 (IL-6) production, with an IC_{50} value of 13.53 μM. Compound **17** showed the most potent anti-inflammatory capacity by inhibiting the LPS-induced generation of nitric oxide (NO) (IC_{50}: 10.86 μM) and interleukin-1β (IL-1β) (IC_{50}: 23.9 μM) and by significantly suppressing induced nitric oxide synthase (iNOS) and phosphorylated nuclear factor-kappa B inhibitor-α (*p*-IκB-α) expression at concentrations of 5 μM and 20 μM, respectively ($p < 0.01$). The modes of interactions between the isolated compounds and the target inflammation-related proteins were investigated in a preliminary molecular docking study. These results provided insight into the chemodiversity and potential anti-inflammatory activities of metabolites with small molecular weights in the mushroom *D. indusiata*.

Keywords: *Dictyophora indusiata*; structure elucidation; sesquiterpenoids; ergosterol derivatives; anti-inflammatory activity; molecular docking

1. Introduction

Dictyophora indusiata, belonging to the family *Phallaceae* (phylum Basidiomycetes) of the Agaricomycetes class of fungi, is famous for its beautiful morphological features. Due to its delicious taste, distinctive fragrance, and medicinal properties, *D. indusiata* has a long history as a healthy food and as a component of folk medicine [1]. Traditional Chinese medicine has widely recognized that *D. indusiata* benefits some chronic diseases by alleviating inflammatory symptoms [2,3]. It is reasonable to suppose the existence of metabolites in *D. indusiata* that offer therapeutic potential.

Most studies on the molecular basis of the nutritional and medicinal values of *D. indusiata* have focused on fungal biomacromolecules, such as carbohydrates and proteins. Polysaccharides are found in the highest concentrations in the mature fruiting body of *D. indusiata* and, therefore, are the most intensively studied chemical constituents of *D. indusiata* [4].

It has been proven that *D. indusiata* polysaccharides (DIPs) have effective anti-tumor, anti-oxidative, anti-inflammatory, immune-enhancing, and anti-diabetes properties [5]. Compared to the polysaccharides, the bioactive compounds with small molecular weights in *D. indusiata* have not been sufficiently investigated [1]. From this mushroom species, three eudesmane-type sesquiterpenes and five monoterpene alcohols were reported to be identified by Kawagishi et al. [6,7]; albaflavenone and two derivatives (9,10-dihydroxy-albaflavenone and 5-hydroxy-albaflavenone) were isolated by Huang et al. and Zhang et al., respectively [8,9]; two linear sesquiterpene carboxylic acids (Phallac acids A and B) were obtained and determined by Lee et al. [10]. In addition to the terpenoid compounds, Lee et al. identified three alkaloids, Dictyoquinazols A, B, and C, from *D. indusiata* [11]; and Sharma et al. reported the isolation of 5-hydroxymethyl–2-furfural (HMF) [12]. The biological investigations revealed that some of these small molecules isolated from *D. indusiata* possess neuroprotective, anti-tyrosinase, anti-glucosidase, and some anti-inflammatory activities [6,9–12]. However, the role of small-molecular-weight metabolites in the anti-inflammatory property of the mushroom *D. indusiata* has yet to be fully elucidated.

Inflammation is a natural response of the immune system to damage from physical, chemical, and pathogenic factors. The activation of the nuclear factor kappa-light-chain-enhancer of activated B cells (NF-κB) pathway plays a central role in acute and chronic inflammation [13]. Abnormally high NF-κB activity is highly associated with aberrant expressions of a series of inflammatory cytokines and other mediators, and it is further associated with many diseases, such as cancer, diabetes, Alzheimer's disease, and cardiac diseases. It has been revealed that the efficient strategy for alleviating inflammatory symptoms involves either reducing the expression of inflammatory cytokines via mediation of the related signaling pathways or by inhibiting their actions using antibodies. In the clinical therapies used to cure inflammatory disease, several cytokine inhibitors, such as Etanercept, Adalimumab, and Infliximab, have been successfully applied. However, the high costs and the side effects of adverse immunological reactions limit their applications [14]. Hence, the discovery of safe and efficacious anti-inflammatory agents is still in urgent demand.

Edible and medicinal fungi are currently seen as important sources of active pharmaceutical ingredients, which can serve as lead molecules in the development of novel drugs. In this context, numerous types of bioactive natural products have been isolated from various fungi [15–17]. In the literature, it is abundantly clear that the anti-inflammatory effect of *D. indusiata* polysaccharides has long been recognized [5,18–20]. However, the potential anti-inflammatory capacity and underlying mechanism of other ingredients in *D. indusiata* are still unclear. Herein, we report on the systematical isolation and identification of the chemical constituents in the ethanolic extract of *D. indusiata*. The inhibitory effects of the isolated compounds against lipopolysaccharide (LPS)-induced inflammatory responses in mouse BV-2 microglial cells were evaluated, and their anti-inflammatory mechanisms of action were investigated using molecular docking simulations. The results of this study might contribute to the knowledge of the chemistry of *D. indusiata* and the discovery of fungal natural products possessing potent anti-inflammatory efficiency with reliable safety profiles.

2. Results

2.1. Structure Elucidation of the Isolated Compounds

Eighteen compounds were isolated from the ethyl acetate partitioned *Dictyophora indusiata* ethanolic extract. On the basis of the comprehensive analysis of spectroscopic data from high resolution electrospray ionization mass spectra (HRESIMS), 1D/2D nuclear magnetic resonance (NMR) spectra, ultraviolet (UV) spectra, and comparison with the references, four previously undescribed compounds were named Indusiataines A–D (**1**–**4**). Fourteen known compounds were elucidated to be 5-(Methoxymethyl)-1*H*-pyrrole-2-carbaldehyde (**5**) [21], nicotinic acid (**6**) [22], dibutyl phthalate (**7**) [23], 5-hydroxymethyl-2-furancarboxaldehyde (**8**) [24], adenosine (**9**) [25], oxindole (**10**) [26], 3-oxo-4-benzyl-3,4-dihydro-1*H*-pyrrolo [2,1-c] oxazine-6-methylal (**11**) [27], 2-methyl-3-pyridinol (**12**) [28], linoleic acid (**13**) [29], oleic acid

(**14**) [30], 1(10→6)abeo-ergosta-5,7,9,22-tetraen-11β-methoxy-3α-ol (**15**) [31], citreoanthras-teroid (**16**) [31], 5α,6α-epoxy-3β-hydroxy-(22*E*)-ergosta-8(14),22-dien-7-one (**17**) [32], and 7-ketositosterol (**18**) [33] (Figure 1). The UV, HRESIMS, and NMR spectra of compounds **1–4** are provided in Figure S1.
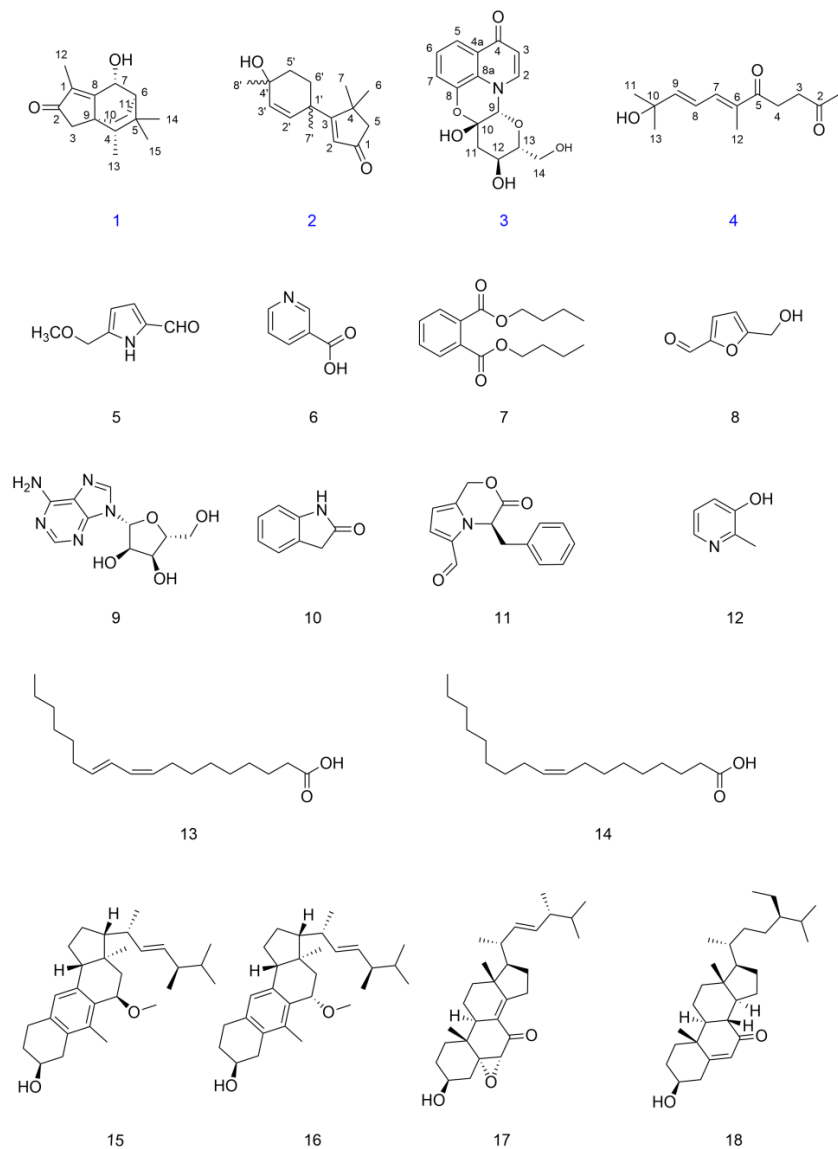

Figure 1. Structures of compounds **1–18** isolated from *Dictyophora indusiata*. The blue color indicates the newly identified compounds.

Compound **1** was obtained as a yellowish amorphous powder. Its molecular formula, $C_{15}H_{22}O_2$, was established by positive HRESIMS (*m/z* 235.1690 [M + H]$^+$, calculated 235.1693), with an index of hydrogen deficiency (IHDs) of five. The UV spectrum of **1** exhibited an absorption maximum of 248.7 nm (Figure S1). The NMR data are provided in Table 1, chemical shifts (*δ*) are reported in parts per million (ppm), and coupling constants (*J*) are given in Hz. The ^{1}H NMR data of compound **1** demonstrated three methine hydrogen signals at δ_H 4.82 (1H, *s*), δ_H 1.36 (1H, *m*), and δ_H 1.14 (1H, *m*); three methylenes at δ_{Ha} 2.08 (1H, *d*, *J* = 18.0) and δ_{Hb} 1.86 (1H, *d*, *J* = 18.0), δ_{Ha} 1.91 (1H, *m*) and δ_{Hb} 0.98 (1H, *m*), and δ_{Ha} 1.78 (1H, *m*) and δ_{Hb} 1.58 (1H, *m*); and four methyls at δ_H 1.69 (3H, *s*), δ_H 0.94 (6H, *d*, *J* = 1.5), and δ_H 0.86 (3H, *d*, *J* = 7). The ^{13}C-NMR spectrum and DEPT spectrum revealed the resonances of 15 carbons (Table 1), which included one ketone carbon (δ_C 208.4), two olefinic carbons (δ_C 181.5 and 132.9), two quaternary carbons (δ_C 45.2 and 34.0), three

methines (δ_C 65.1, 46.8, and 43.6), three methylenes (δ_C 44.7, 25.4, and 16.6), and four methyls (δ_C 30.3, 25.2, 11.6, and 8.5). The other eleven carbons and the unassigned three IHDs suggested that compound **1** possessed a tricyclic core group. A cyclopentenone ring (ring A, which contained C-1, C-2, C-3, C-8, and C-9) was furnished by the HMBC correlations (Figure 2) of H-3 (δ_H 2.08 and 1.86) to C-1 (δ_C 132.9), C-2 (δ_C 208.4), C-8 (δ_C 181.5), and C-9 (δ_C 45.2), and from H-12 (δ_H 1.69) to C-1, C-2 and C-8. The ^{1}H-^{1}H COSY correlations of H-10 (δ_H 1.91, 0.98)/H-11 (δ_H 1.78, 1.58), H-11/H-6 (δ_H 1.36), and H-6/H-7 (δ_H 4.82) suggested that the connections were C-10 (δ_C 25.4) to C-11 (δ_C 16.6), C-11 to C-6 (δ_C 46.8), and C-6 to C-7 (δ_C 65.1). In combination with HMBC correlations from H-6 (δ_H 1.36) to C-8, H-3 to C-10 (δ_C 25.4), and 7-OH (δ_H 5.19) to C-8 indicated that C-8 and C-9 were involved in further cyclization, leading to a cyclohexane ring (ring B) fused to ring A at C-8 and C-9; ring B was composed of C-6, C-7, C-8, C-9, C-10, and C-11. HMBC correlations of H-13 (δ_H 0.86) with C-5 (δ_C 34.0), C-9 (δ_C 45.2), and H-14,15 (δ_H 0.94) with C-6 suggested that C-6 and C-9 were the bridgehead carbons of another cyclohexane ring (ring C), which contained C-4, C-5, C-6, C-7, C-8, and C-9. Furthermore, four methyls at H-12, H-13, H-14, and H-15, along with HMBC correlations of H-12/C-1, H-13/C-4, and H-14, 15/C-5, confirmed the connection of the methyl group. Compound **1** was finally established, as depicted in Figure 1, with a fused tricyclic system comprised of a cyclopentenone (ring A) and two cyclohexane (rings B and C) fragments. The relative configuration was further deduced from ROESY data (Figure 2), and key correlations between H-10 and H-13 and between H-7 and H-14 or -15 suggested that H-10, H-11, H-13, and 7-OH were on the same face of ring B. Thus, the relative configuration for compound **1** could be considered a pair of enantiomers of 4*R′*,6*S′*,7*S′*,9*S′*. TD-DFT ECD calculations confirmed the absolute configuration of compound **1**, and the structure was optimized by functional analysis of ωB97XD with the TZVP basis set and MeOH as SMD. The obtained calculated ECD spectra (Figure 3) of (4*S*,6*R*,7*R*,9*R*)-9b showed a complete match to the measured spectrum. The absolute configuration of compound **1** was further confirmed by single-crystal X-ray diffraction with a suitable Flack parameter of 0.04 (Figure 4). The absolute configuration of compound **1** was determined to be 4*S*,6*R*,7*R*,9*R*, and it was named Indusiataine A.

Table 1. ^{1}H and ^{13}C-NMR spectroscopic data (DMSO-*d6*, 500/125 MHz) for compounds **1–4**.

Compound 1			Compound 2			Compound 3			Compound 4		
no	δ_C	δ_H, multi., *J*	no	δ_C	δ_H, multi., *J*	no	δ_C	δ_H, multi., *J*	no	δ_C	δ_H, multi., *J*
1	132.9		1	206.8		2	143.3	8.03, *d*, 7.5	1	30.3	2.12, *s*
2	208.4		2	129.3	5.88, *s*	3	110.5	6.14, *d*, 7.5	2	207.9	
3	44.7	2.08, 1.86, *d*, 18.0	3	193.5		4	177.4		3	37.5	2.66, *t*, 6.0
4	43.6	1.14, *m*	4	44.9		4a	126.5		4	31.4	2.92, *t*, 6.0
5	34.0		5	54.8	2.25, *d*, 11.0	5	117.9	7.68, *dd*, 9.0, 1.5	5	200.1	
6	46.8	1.36, *m*	6	28.5	1.34, *s*	6	124.4	7.28, *t*, 9.0	6	134.3	
7	65.1	4.82, *s*	7	29.4	1.26, *s*	7	118.8	7.24, *dd*, 9.0, 1.5	7	139.1	7.23, *d*, 11.5
8	181.5		1′	41.4		8	143.4		8	122.0	6.58, *d*, 15.0, 11.5
9	45.2		2′	132.9	5.72, *dd*, 10.0, 1.0	8a	127.0		9	152.4	6.37, *d*, 15.0
10	25.4	1.91, 0.98, *m*	3′	135.1	5.56, *dd*, 10.0, 1.0	9	85.0	5.40, *s*	10	70.0	
11	16.6	1.78, 1.58, *m*	4′	66.2		10	93.1		11	30.2	1.24, *s*
12	8.5	1.69, *s*	5′	35.3	1.61, 1.40, *m*	11	43.7	2.64, *dd*, 11.5, 5.0; 1.85, *dd*, 13.0, 6.0	12	12.0	1.79, *s*
13	11.6	0.86, *d*, 7.0	6′	34.3	1.92, 1.74, *m*	12	63.2	3.59, *m*	13	30.2	1.24, *s*
14	30.3	0.94, *s*, 1.5	7′	29.9	1.28, *s*	13	82.8	3.48, *m*			
15	25.2	0.94, *s*, 1.5	8′	29.5	1.10, *s*	14	60.9	3.65, *d*, 11.5; 3.42, overlap			
7-OH		5.19, *d*, 6.0	4′-OH		4.55, *s*						

DMSO-*d6*: deuterated dimethyl sulfoxide. Internal reference standard: tetramethylsilane (TMS). Chemical shifts (δ) are recorded in parts per million (ppm), and coupling constants (*J*) are given in Hz.
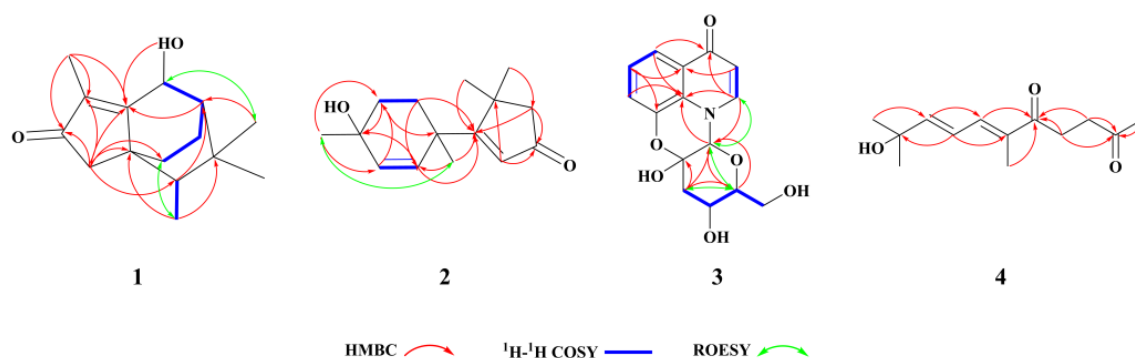
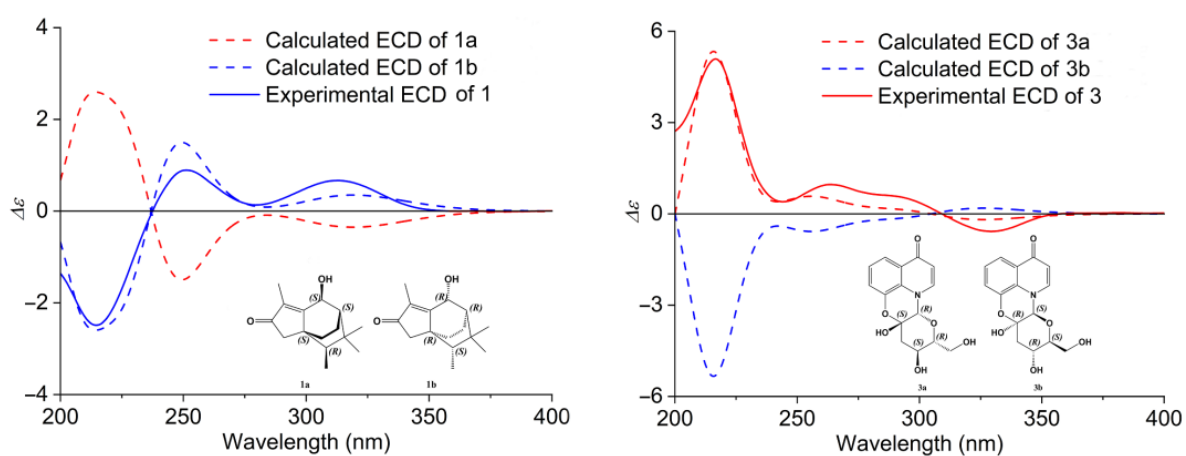**Figure 2.** Key HMBC, COSY, and ROESY correlations of compounds **1**–**4**.

Figure 3. The experimental ECD spectra and calculated ECD curves of compounds **1** and **3**.
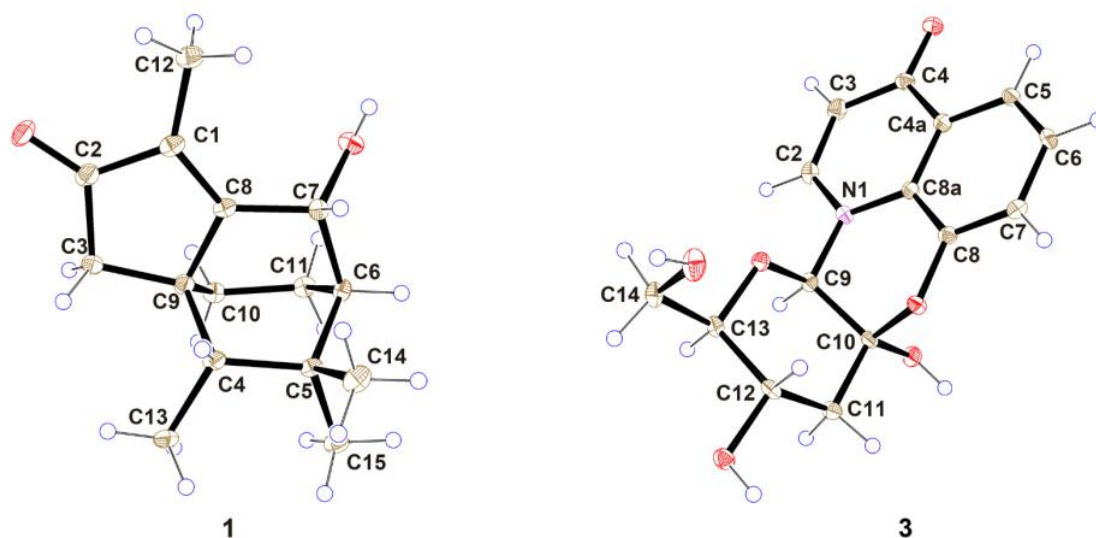

Figure 4. ORTEP (Oak Ridge Thermal-Ellipsoid Plot Program) plots of the X-ray crystal structure of compounds **1** and **3**. Ellipsoids are drawn at the 35% probability level.

Compound **2** was purified as a yellowish oil. Its molecular formula, $C_{15}H_{22}O_2$, was established by positive HRESIMS (*m/z* 235.1694 [M + H]$^+$, calculated 235.1693), with an index of hydrogen deficiency (IHDs) of five. The UV spectrum exhibited an absorption maximum of 235.7 nm (Figure S1). The ^{1}H NMR spectrum (Table 1) displayed signals for two double bonds, which included three hydrogen signals at δ_H 5.88 (1H, *s*), δ_H 5.72

(1H, *dd*, *J* = 10.0, 1.0), and δ_H 5.56 (1H, *dd*, *J* = 10.0, 1.0); three methylenes at δ_H 2.25 (2H, *d*, *J* = 11.0), δ_{Ha} 1.92 (1H, *m*) and δ_{Hb} 1.74 (1H, *m*) and at δ_{Ha} 1.61 (1H, *m*) and δ_{Hb} 1.40 (1H, *m*); and four methyls at δ_H 1.34 (3H, *s*), δ_H 1.28 (3H, *s*), δ_H 1.26 (3H, *s*), and δ_H 1.10 (3H, *s*) in the ^{1}H NMR spectrum as well as active hydrogen signals at δ_H 4.55 (1H, *s*). The ^{13}C-NMR and DEPT spectra (Table 1) showed carbon signals corresponding to the chemical units described above and confirmed their presence. These resonances included one ketone carbon (δ_C 206.8), three olefinic carbons (δ_C 135.1, δ_C 132.9, and δ_C 129.3), and three odd numbers, which indicated that δ_C 193.5 prefers one olefinic carbon, not to a ketone carbon; three quaternary carbons (δ_C 66.2, δ_C 44.9, and δ_C 41.4), three methines (δ_C 54.8, δ_C 35.3 and δ_C 34.3), and four methyl carbons (δ_C 29.9, δ_C 29.5, δ_C 29.4, and δ_C 28.5). In the HMBC spectrum (Figure 2), correlations of H-2 (δ_H 5.88) to C-4 (δ_C 44.9), C-5 (δ_C 54.8), and C-1 (δ_C 206.8) and from H-5 (δ_H 2.25) to C-1 (δ_C 206.8) and C-3 (δ_C 193.5), suggesting that a cyclopentenone (ring A) was formed by C-1, C-2 (δ_C 129.3), C-3, C-4, and C-5; a cyclohexene ring (ring B) formed by C-1′ (δ_C 41.4), C-2′ (δ_C 132.9), C-3′ (δ_C 135.1), C-4′ (δ_C 66.2), C-5′ (δ_C 35.3), and C-6′ (δ_C 34.3) was readily furnished by the ^{1}H-^{1}H COSY correlations (Figure 2) of H-2′ (δ_H 5.72)/H-3′ (δ_H 5.56) and H-5′ (δ_H 1.61, 1.40)/H-6′ (δ_H 1.92, 1.72), in combination with HMBC correlations of H-2′, H-3′, H-5′ (δ_H 1.61, 1.40) and H-6′ (δ_H 1.92, 1.74) to C-1′ and C-4′. HMBC correlations of H-6 (δ_H 1.34) and H-7 (δ_H 1.26) with C-3 and C-5, H-7′ (δ_H 1.28) with C-3 and C-2′, and H-8′ (δ_H 1.10) with C-3′ and C-5′, which indicated four methyl positions, as depicted in Figure 2, respectively. The relative configuration was further deduced from ROESY data (Figure 2). Key correlations between H-7′ and H-8′ suggested that H-7′ and H-8′ were on the same face of ring B. Therefore, a pair of enantiomers of 1′*S*′, 4′*R*′ was possible for the relative configuration of compound **2**. The relative configuration of compound **2** was established as 1′*S*, 4′*R*, and named Indusiataine B.

Compound **3** was isolated as a brown oil, and after recrystallization in methanol, dark brown needle-shaped crystallites were obtained. Compound **3** afforded a molecular formula of $C_{15}H_{15}NO_6$, as evidenced by negative HRESIMS (*m/z* 306.0981 [M − H]$^-$, calculated 306.0972), with an index of hydrogen deficiency (IHDs) of nine. The UV spectrum exhibited an absorption maximum of 229.8 nm (Figure S1). The ^{1}H NMR spectrum (Table 1) displayed five aromatic protons at δ_H 8.03 (1H, *d*, *J* = 7.5), δ_H 7.68 (1H, *dd*, *J* = 9.0, 1.5), δ_H 7.28 (1H, *t*, *J* = 9.0), δ_H 7.24 (1H, *dd*, *J* = 9.0, 1.5), and δ_H 6.14 (1H, *d*, *J* = 7.5); one hydroxy group at δ_H 5.40 (1H, *s*); two oxygenated methines at δ_H 3.59 (1H, *m*) and δ_H 3.48 (1H, *m*); and one oxygenated methylene at δ_{Ha} 3.65 (1H, *d*, *J* = 11.5) and δ_{Hb} 3.42 (1H, overlap); and one methylene at δ_{Ha} 2.64 (1H, *dd*, *J* = 11.5, 5.0) and δ_{Hb} 1.85 (1H, *dd*, *J* = 13.0, 6.0). Using DEPT and HSQC spectra, fifteen carbon resonances displayed in the ^{13}C-NMR (Table 1) were assigned to one ketone carbon (δ_C 177.4); eight olefinic carbons (δ_C 143.4, 143.3, 127.0, 126.5, 124.4, 118.8, 117.9, and 110.5); an oxygenated quaternary carbon (δ_C 93.1); three oxygenated tertiary carbons (δ_C 85.0, 82.8, and 63.2); and two methylenes (δ_C 60.9 and 43.7). The ^{1}H-^{1}H COSY correlation (Figure 2) of H-5 (δ_H 7.68)/H-6 (δ_H 7.30)/H-7 (δ_H 7.24) and H-2(δ_H 8.03)/H-3(δ_H 6.14), along with HMBC correlations (Figure 2) of H-5 to C-8*a* (δ_C 127.0) and C-4 (δ_C 177.4), H-6 to C-4*a* (δ_C 126.5) and C-8 (δ_C 143.4), H-7 to C-8*a*, H-3/C-4*a* and H-2 to C-4 and C-8*a* indicated the existence of the characteristic 8-substituted-4-quinolone. Considering the remaining two unassigned IHDs, the rest of the group contained two rings. A tetrahydropyran ring was furnished by the HMBC correlations from H-11 (δ_H 2.46, 1.85) to C-9 (δ_C 85.0) and C-10 (δ_C 93.1) and from H-9 (δ_H 5.40) to C-13 (δ_C 82.8), in combination with the ^{1}H-^{1}H COSY correlations of H-11/H-12 (δ_H 3.85) and H-12/H-13 (δ_H 3.85). The key HMBC interactions of H-2/C-9 and H-9/C-8*a* and the downfield shifts of C-8, C-9, and C10 indicated that N-1, C-8*a*, C-8, C-9, and C-10 generated a morpholine ring. Furthermore, the ^{1}H-^{1}H COSY correlation H-13/H-14 (δ_H 3.67, 3.42) confirmed the connection between C-13 and C-14. Thus, the 2D structure of compound **3** was established. The relative configuration of compound **3** was confirmed by the ROESY spectrum (Figure 2), key correlations between H-9 and H-13, and between H-11 and H-13; and no correlation between H-12 and H-13 suggested that H-9 and H-13 were on the same side, but H-12 was on the opposite side. Therefore, the relative configuration of compound **3** could be

9*R*′,10*S*′,12*S*′,13*R*′. The absolute configuration of compound **3** was confirmed by ECD measurement and comparison with the calculated TD-DFT ECD data through the structure optimization by functional analysis of ωB97XD with the TZVP basis set and MeOH as SMD. The ECD calculation was performed after the optimization of conformers 5-a and 5-b. The comparison of the experimental and theoretically calculated ECD curves (Figure 3) confirmed the assignment of the absolute configuration of compound **3** as 9*R*,10*S*,12*S*,13*R*. The absolute configuration of compound **3** was also established by single-crystal X-ray diffraction with a suitable Flack parameter of −0.04 (Figure 4). The absolute configuration of **3** was determined to be 9*R*,10*S*,12*S*,13*R*, and it was named Indusiataine C.

Compound **4** was purified as a yellowish oil, and its molecular formula, $C_{13}H_{20}O_3$, was determined by positive HRESIMS (*m/z* 225.1482 [M + H]$^+$, calculated 225.1485) with an index of hydrogen deficiency (IHDs) of four. The UV spectrum of compound **4** displayed an absorption maximum of 277.1 nm (Figure S1). The ^{1}H NMR spectrum (Table 1) indicated the presence of two *trans*-conjugated double bonds, as supported by hydrogen signals at δ_H 7.23 (1H, *d*, *J* = 11.5), δ_H 6.58 (1H, *dd*, *J* = 15.0, 11.5), and δ_H 6.37 (1H, *d*, *J* = 15.0). Additionally, two methylenes at δ_H 2.92 (2H, *t*, *J* = 6.0) and δ_H 2.66 (2H, *t*, *J* = 6.0); four methyls at δ_H 2.12 (3H, *s*), δ_H 1.79 (3H, *s*), and δ_H 1.24 (6H, *s*) were observed in the ^{1}H NMR spectrum as well as active hydrogen signals at δ_H 4.86 (1H, *s*). The ^{13}C-NMR spectrum revealed the resonances of 13 carbons (Table 1). Based on the DEPT spectrum, these resonances included two ketone carbons (δ_C 207.9 and δ_C 200.1), four olefinic carbons (δ_C 152.4, δ_C 139.1, δ_C 134.3, and δ_C 122.0), one quaternary carbon (δ_C 70.0), two methylenes (δ_C 37.5 and δ_C 31.4), and four methyl carbons (δ_C 30.3, δ_C 30.2, δ_C 30.2, and δ_C 12.0). The degree of unsaturation of compound **4** was calculated as 4, indicating that it had a linear structure. In the HMBC spectrum (Figure 2), correlations of H-1 (δ_H 2.12), H-3 (δ_H 2.66), H-4 (δ_H 2.92) to C-2 (δ_C 207.9) and correlations of H-3, H-4, and H-7 (δ_H 2.92) to C-5 (δ_C 200.1) were observed; the conjugated diene at H-7, H-8, and H-9 along with correlations of H-8 (δ_H 6.58)/C-6 (δ_C 134.3), H-9 (δ_H 6.37)/C-7 (δ_C 139.1), and H-8/C-10 (δ_C 70.0) and correlations of two methyls from H-11,12 (δ_H 1.24) to C-9 (δ_C 152.4) confirmed the two-dimensional (2D) structure of compound **4**. Thus, the structure of compound **4** was determined to be an acyclic norsesquiterpenoid and named Indusiataine D.

2.2. Biological Activity

Numerous fungal metabolites have been reported to have anti-inflammatory activities [34,35]. According to the structural information of these reported compounds and based on our research interests, compounds **1**, **3**, **4**, **11**, **15**, **16**, and **17** were selected for further biological evaluations.

2.2.1. Effects of the Compounds on Cell Viability

The cytotoxicity of compounds **1**, **3**, **4**, **11**, **15**, **16**, and **17** on BV-2 cells was evaluated using a thiazolyl blue tetrazolium bromide (MTT) assay [36]. As shown in Figure 5, after 24 h of exposure, the tested compounds at the examined concentrations did not induce significant cytotoxicity in the BV-2 cells (*p* > 0.05); therefore, subsequent in vitro anti-inflammatory experiments were performed with these concentrations.

2.2.2. Effects of the Compounds on NO Production in LPS-Stimulated BV-2 Cells

During inflammation, the induced nitric oxide synthase (iNOS) would be activated and produce large amounts of nitric oxide (NO) [37]. The inhibitory effects of the selected compounds on NO production in LPS-induced microglia BV-2 cells were evaluated by measuring the nitrite content accumulated in the culture medium based on the Griess reaction [38]. Among the tested compounds (Table 2), compound **17** exhibited the most potent inhibitory effect against LPS-induced NO production in the BV-2 cells, with an IC$_{50}$ of 10.86 μM, followed by another sterol compound, compound **15** (IC$_{50}$: 42.41 μM). Compound **16** was the epimer of compound **15**; however, its IC$_{50}$ value was 66.12 μM, indicating a comparatively weak inhibitory capacity. The IC$_{50}$ values of three tested

previously undescribed compounds, compounds **1**, **3**, and **4**, were 46.30 μM, 89.12 μM, and 62.15 μM, respectively. Moreover, compound **11** possessed no NO production inhibitory activity at the tested concentrations.
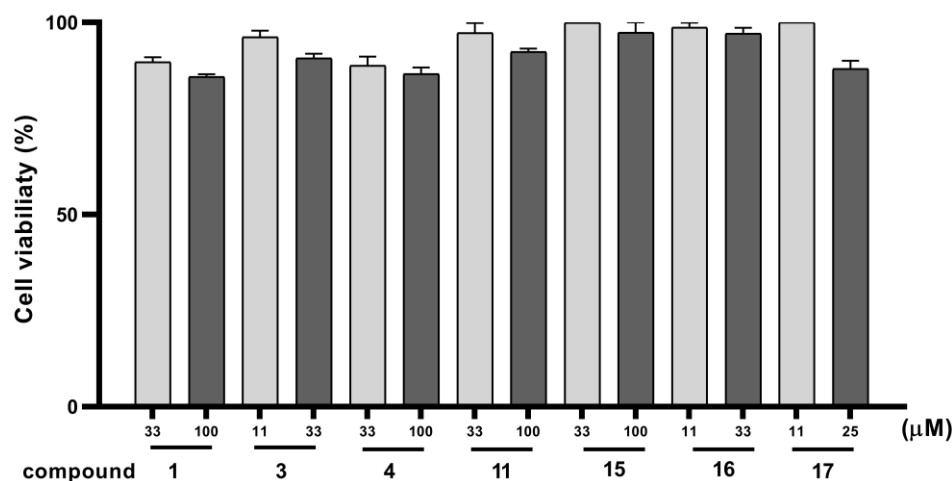

Figure 5. Effects of compounds **1**, **3**, **4**, **11**, **15**, **16**, and **17** at different concentrations on BV-2 cell viability. Cell viability was evaluated by thiazolyl blue tetrazolium bromide (MTT) assay. The results are represented by a percentage of examined viability of the normal cell group (where the cells were cultured under the normal growth condition), was set as 100%, and are expressed as the mean of triplicates; error bars indicate standard deviations (SD).

Table 2. In vitro inhibitory activities of compounds **1**, **3**, **4**, **11**, **15**, **16**, and **17** against LPS-stimulated production of pro-inflammatory mediators in BV-2 cells.

Compounds	Pro-Inflammatory Mediators (IC$_{50}$ in μM)			
	NO	**TNF-α**	**IL-1β**	**IL-6**
1	46.3 ± 1.35	34.5 ± 2.1	>100	77.57 ± 4.43
3	89.12 ± 8.54	11.9 ± 1.25	>100	46.34 ± 2.34
4	62.15 ± 4.64	>100	>100	>100
11	>100	86.2 ± 6.33	>100	58.43 ± 2.23
15	42.41 ± 3.44	65.5 ± 1.45	>100	49.43 ± 2.15
16	66.12 ± 4.38	>100	>100	13.53 ± 1.46
17	10.86 ± 0.73	>100	23.9 ± 1.48	>100

Results are presented as 50% inhibitory concentration (IC$_{50}$) values in μM. The LPS-stimulated production of pro-inflammatory mediators in the LPS-treated group (where the cells were treated with LPS but without compounds) was set as 100%. All measurements were carried out in triplicates. Data are mean value $\pm$ standard deviation. LPS: lipopolysaccharide. NO: nitric oxide. TNF-α: tumor necrosis factor-α. IL: interleukin.

2.2.3. Effects of the Compounds on Levels of TNF-α, IL-1β, and IL-6 in LPS-Stimulated BV-2 Cells

To examine the inhibitory effects of the selected compounds on the LPS-induced production of pro-inflammatory cytokines, we investigated the levels of tumor necrosis factor-α (TNF-α), interleukin-1β (IL-1β), and interleukin-6 (IL-6) in LPS-treated BV-2 cells using ELISA. As shown in Table 2, the treatments with compounds **1**, **3**, **11**, and **15** exhibited inhibitions of TNF-α production. Among them, compound **3** had the strongest inhibitory activity (IC$_{50}$: 11.9 μM). The expression of LPS-induced IL-1β could be only inhibited by compound **17**, with an IC$_{50}$ value of 23.9 μM. Regarding the LPS-induced generation of IL-6, the inhibitory effects of compounds **1**, **3**, **11**, **15**, and **16** were observed, and compound **16** displayed the lowest IC$_{50}$ value of 13.53 μM.

2.2.4. Effects of the Compounds on Expressions of iNOS and p-IκB-α in LPS-Stimulated BV-2 Cells

A Western blot analysis was employed to further determine the inhibitory effects of the selected compounds on two key enzymes involved in the inflammatory response: iNOS and phosphorylated nuclear factor-kappa B inhibitor-α (p-IκB-α) [39]. Figure 6A,B show that compounds **15** and **17** significantly reduced iNOS expression at concentrations of 20 μM ($p < 0.05$) and 5 μM ($p < 0.01$), respectively. This finding is consistent with the results of the previous assay, where compounds **15** and **17** possessed the highest NO production inhibition activity. As shown in Figure 6C, compound **17** significantly inhibited p-IκB-α expression ($p < 0.01$). The treatments with the other tested compounds exhibited no or weak effects on the levels of iNOS and p-IκB-α, with no statistical differences (Figure S2).
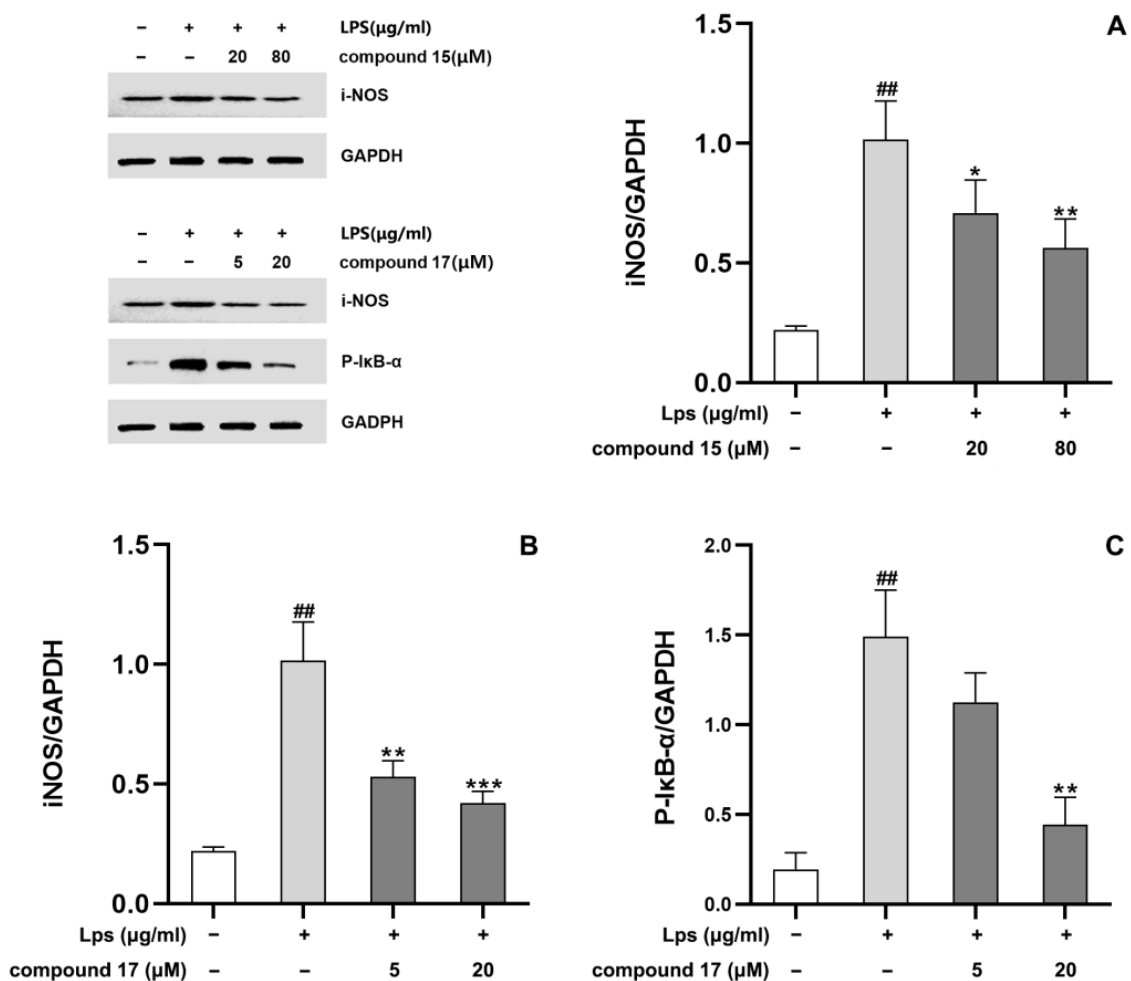

Figure 6. Significant alleviation of increased expression of inflammation-related proteins in lipopolysaccharide (LPS)-simulated BV-2 cells, following the treatments of compounds **15** and **17** with indicated concentrations. (**A**): compound **15** against iNOS expression. (**B**): compound **17** against iNOS expression. (**C**): compound **17** against p-IκB-α expression. The results are presented as the mean of triplicates; error bars indicate standard deviations. ## $p < 0.01$ for comparisons with the normal cell group, where the cells were cultured under the normal growth condition. * $p < 0.05$, ** $p < 0.01$, and *** $p < 0.001$ for comparisons with the LPS-treated group, where the cells were treated with LPS but without compounds.

2.3. Molecular Docking Simulation

A molecular docking study was conducted based on the results obtained from the previous in vitro experiments to further explore the anti-inflammatory mechanisms of the selected compounds.

As compounds **15** and **17** exhibited good inhibitory activity on the LPS-induced generation of NO and the expression of iNOS in the BV-2 cells, a molecular docking study was performed to clarify their modes of interactions with iNOS. As shown in Figure 7A,B, the binding of compounds **15** and **17** with iNOS was achieved by stacking the compounds over the active region of haem and forming hydrogen bonds with the iNOS protein backbone [40]; both compounds fitted well within this pocket, with compound **15** forming three hydrogen bonds with Gln257, Pro334, and Gly365 (binding energy: −8.21 kcal/mol) and compound **17** establishing three hydrogen bonds with Glu257, Gly365, and Tyr367 (binding energy: −7.29 kcal/mol).
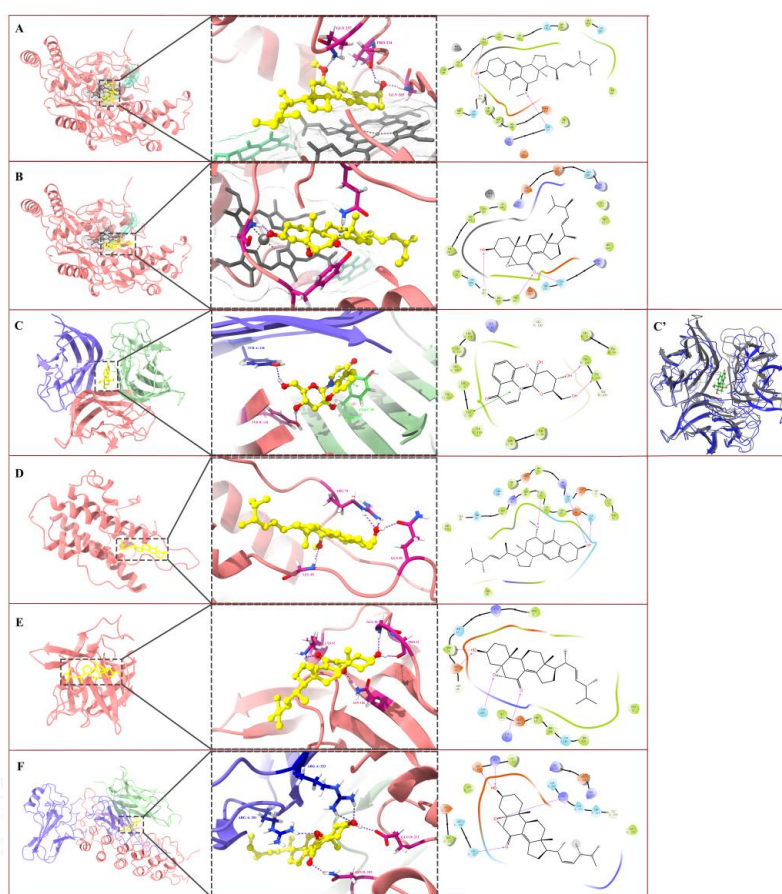

Figure 7. Molecular docking results of compounds **3**, **15**, **16**, and **17** with target inflammation-related proteins. (**A**): compound **15** with iNOS. (**B**): compound **17** with iNOS. (**C**) and (**C′**): compound **3** with TNF-α. (**D**): compound **16** with IL-6. (**E**): compound **17** with IL-1β. (**F**): compound **17** with IκB-α/NF-κB complex. For clarity, only interacting residues are labeled. In the three-dimensional representations, compounds are shown in the ball and stick model: yellow, carbon; red, oxygen; blue, nitrogen; white, hydrogen. Hydrogen bonding interactions are shown by purple dashes, and pi-interactions are shown by green dashes. In (**A**) and (**B**): black, haem molecule. In (**C**): purple, chain A; pink, chain B; cyan, chain C. In (**C′**): black, the original conformation of TNF-α; blue, the conformation of TNF-α formed after docking with compound **3**. In (**F**): purple, chain A; cyan, chain C; pink, chain D. In the two-dimensional representations, hydrogen bonding interactions are shown by purple arrows, arrows denote hydrogen bonds; pi-interactions are shown by green lines. Residues shown in green discs indicate hydrophobic interactions.

The compounds shown to have strong bio-activities in the ELISA tests were subjected to molecular docking studies with the corresponding pro-inflammatory cytokines. TNF-α has three identical receptor binding sites, as the protein possesses a unique threefold symmetry structure [41]. Compound **3** docked flexibly into the hydrophobic pocket located in the trimer core with a binding energy of −8.53 kcal/mol (Figure 7C). The three main binding interactions were the hydrogen bond established between the hydroxyl groups at C-14 with Tyr118 residues on chain A, the hydrogen bond established between the hydroxyl groups at C-12 with Tyr118 residues on chain B, and Pi-Pi stacking from the 4-pyridone ring with Tyr59 residues on chain C. Visible conformational changes in TNF-α occurred after the docking of compound **3**, the helices on chains A and B disappeared, and a large number of loop structures newly formed (Figure 7C′). Therefore, it was speculated that compound **3** inhibited TNF-α function by changing the protein structure and disrupting the receptor binding sites. Compound **16** bounded to two loop structures of IL-6 (Figure 7D) by forming three hydrogen bonds with Arg74, Leu89, and Gln85 (binding energy: −8.39 kcal/mol). Compound **17** matched well in the protein-binding pocket with IL-1β (Figure 7E); it formed four hydrogen bonds with Glu50, Pro51, Lys97, and Asn102 of IL-1β with a binding energy of −4.40 kcal/mol.

The IκB-α/NF-κB complex used for this molecular docking study is composed of three subunits [42]: NF-κB-P65 (chain A), NF-κB-P50 (chain C), and IκB-α (chain D) (Figure 7F). Compound **17** could be bound to the lower part of the central cavity of the complex and interacted with NF-κB-P65 (chain A) and IκB-α (chain D) (binding energy: −4.49 kcal/mol). The primary binding interactions were the hydrogen bonds formed between the hydroxyl group with Arg253 residues on chain A and Glu213 on chain D, the hydrogen bond established between the epoxy group and Arg201 on chain A, and the hydrogen bond formed between the carbonyl oxygen and Asn182 on chain D.

3. Discussion

3.1. Diversity of Metabolites with Small Molecular Weights in D. indusiata

There are four main stages in the morphological development of the fruit body of *D. indusiata*: the primordia stage, the ball-shaped stage, the peach-shaped stage, and the mature stage. An integrated quantitative proteomic and metabolomic analysis has revealed that [43], compared to the three early stages, more metabolites with <15 carbon atoms in the mature fruiting body of *D. indusiata* are upregulated, and for metabolites with ≥15 carbon atoms, more metabolites are downregulated. This phenomenon suggests that, in the final growth stage, large amounts of natural products with comparatively small molecular weights are preferentially biosynthesized and accumulated and that these chemical constituents may be crucial contributors to the taste, fragrance, and nutritional and medicinal properties of the mature fruiting body of *D. indusiata*. Our result is consistent with that reported above. In this research, eighteen small-molecule compounds were isolated from the ethanolic extract of *D. indusiata*, of which the number of core skeleton carbon atoms in **11** isolated compounds were less than **15**.

Among the four compounds newly described in this manuscript, three were terpenoids. Terpenoids are one of the largest groups of secondary metabolites found in nature. Edible fungi are considered prolific producers of structurally diverse terpenoid compounds, as these fungi possess an extensive repertoire of natural product biosynthesis pathways [44,45]. Compound **1** was a tricyclic sesquiterpenoid with a skeleton of antsorane [46,47], compound **2** was a rearranged cuparane-type sesquiterpenoid [48], and compound **4** was an acyclic norsesquiterpenoid [49,50]. The antsorane skeleton contained in compound **1** was quite unusual. As a natural product, antsorenone (synonym antsorane) was first discovered by Chazan in 1969 from the plant *Elionurus tristis* [46]. Several analogs were successively identified from *Eremophila fraseri* [51], *Vetiveria nigritana* [52], and *Chrysopogon zizanioides* [53]. The structure of antsorane was fully characterized by Gabriel P. Garcia et al. in 2019 [47]. To the best of our knowledge, compound **1** is the second natural compound ever reported with this specific sesquiterpenic ketone skeleton and the first one isolated from fungi. In Garcia

et al.'s article, the high stability of the antsorane molecule was found, as it was subjected to several Brönsted and Lewis acid treatments and all the attempts to transform it into zizaen-3-one following a reverse Wagner–Meerwein rearrangement under acidic conditions failed. Accordingly, Garcia et al. hypothesized that the antsorane skeleton was the final step of the biosynthesis pathway that started with acorane. In terms of the molecular structure of our compound **1**, a hydroxyl group was present on the bridged ring of the antsorane skeleton; its formation pathway and its biological role in the ecology and physiology of *D. indusiata* deserve further attention and investigation.

The structural diversity of fungal terpenoids contributes to functional diversity. Terpenoids are widely involved in every aspect of fungi growth, development, and stress responses [45]. Fungal terpenoids play biological signaling and defensive roles, as they often possess a volatile profile and a unique aromatic property [54]; they can mediate many ecological interactions between fungi and other organisms. In this research, we found that compound **1** had a considerable sour and smelly odor, and the newly described compound **3** had an aroma of wood mixed with caramel. Together with the known odorous compounds, such as nicotinic acid (**6**) and oxindole (**10**), these small-molecular-weight compounds are vital contributors to the distinctive fragrance of *D. indusiata*.

According to the classes of the enzyme involved in their biosynthesis, the major groups of fungal secondary metabolites can be classified as polyketides, non-ribosomal peptides, terpenes, and alkaloids [55]; they can serve as metabolic precursors for a wide range of other metabolites. Only a relatively small number of higher fungal species have been chemically investigated; fungal natural products represent a vast and largely untapped source of potentially potent new pharmaceuticals [56,57]. Among fungal species, the basidiomycetes are one of the most important producers of diverse bioactive secondary metabolites [58,59]. *Ganoderma lucidum* and *Poria cocos* are two well-known medicinal basidiomycetes. Based on the phytochemical reports, more than 270 secondary metabolites have been reported to be isolated from *Ganoderma lucidum* [60–62]; more than 140 terpenoids and more than 20 steroids have been identified in *Poria cocos* [63,64]. As reviewed by Habtemariam [1] and described in the Section 1, the small-molecule compounds identified from *D. indusiata* mainly include a few terpenoids and alkaloids. The chemodiversity of this edible and medicinal mushroom species has not been adequately characterized. In this study, various terpenoids, steroids, lactones, fatty acids, and heterocyclic compounds were identified. The present findings reveal that abundant small-molecular-weight metabolites with highly complicated and diverse structures exist in the mushroom *D. indusiata*. These small molecules may form the basis for the further exploitation of *D. indusiata* as a source of functional ingredients for the food, cosmetic, and pharmaceutical industries.

3.2. Ergostane-Type Steroids Isolated from D. indusiata and Their Anti-Inflammatory Activities

The scientific literature on the biological activities of small-molecule metabolites in *D. indusiata* remains very scarce. Only two derivatives of albaflavenone isolated from *D. indusiata* were evaluated for their anti-inflammatory activities; these two compounds showed moderate inhibitory effects on LPS-induced NO production and TNF-*α* secretion in BV-2 cells [9]. In this research, three tested ergostane-type steroids (**15**, **16**, and **17**) isolated from *D. indusiata* exhibited good anti-inflammatory activities. Ergosterol is the primary sterol in fungal membranes and presumably contributes to membrane fluidity and function [65]. Ergosterol and its related derivatives are metabolites essential for fungal growth, development, and adaptation to various stresses [66]. Ergosterol biosynthesis can be divided into three modules: mevalonate, farnesyl pyrophosphate (farnesyl-PP), and ergosterol biosynthesis [67]. Ergosterol and some of its biosynthetic intermediates are critical natural products of great economic value. In the pharmaceutical industry, ergosterol is a direct precursor of vitamin D2 and steroid drugs [68].

Pharmaceutical steroids, non-steroidal anti-inflammatory drugs (NSAIDs), and anti-histamines have been widely applied in anti-inflammatory therapies [69]. In some cases, the marketed anti-inflammatory drugs may not deliver a radical cure and may cause side

effects [70,71]. Therefore, the search for novel and safe anti-inflammatory agents or lead compounds in nature has become the focus of biologists and chemists. The extensive efforts devoted to searching for promising ergostane-type steroid compounds with high anti-inflammatory activities in fungi and to elucidating their mechanisms of action have recently been well-reviewed [34,35,66]. In the present study, the best anti-inflammatory activities (reflected by the smallest IC_{50} values) were exerted by compound **15** against TNF-α production (IC_{50} = 65.5 μM), compound **16** against IL-6 production (IC_{50} = 13.53 μM), and compound **17** against NO and IL-1β production (IC_{50} = 10.86 μM and 23.9 μM, respectively). Moreover, the evident suppression of iNOS and *p*-IκB-α expressions by compound **17** was observed. Since the experimental models vary among the related research, it is not easy to appropriately compare our results to the data reported in the literature.

Nevertheless, comparing the data obtained within our in vitro anti-inflammatory assays and in silico analysis may provide new insights into the structure–activity relationship of isolated sterols. Compounds **15** and **16** were two ergosterol derivatives with a rearranged tetracyclic skeleton [72]; they were epimers, and the stereo configuration of their methoxy at C-11 was on the same face and on the opposite face to the hydroxyl group on their molecules, respectively (Figure 1). Compound **15** showed higher inhibitory activity on LPS-induced NO production than compound **16**. From the visualized results of molecular docking, the hydroxyl group of compound **15** formed a hydrogen bond with Gly365 of iNOS. In addition, the methoxy group, which was on the same face as the hydroxyl group, formed another hydrogen bond with Gln257. Notably, compound **17**, the most potent NO production inhibitor found in this research, also established hydrogen bonds with the amino acid residues of Gly365 and Gln257 of iNOS. It can be deduced that the methoxy and the hydroxyl groups located on the same face of the molecule conferred compound **15** the capacity to interact with Gly365 and Gln257 simultaneously, which was crucial for its inhibitory effect against iNOS. In contrast, compound **16** showed the strongest inhibitory activity against IL-6 production among the tested compounds. The structure of IL-6 contained four relatively long α-helices (A–D) and two short helices (S1 and S2) linked via loop structures [73]. The docking result demonstrated that the binding site of compound **16** was situated in the loop region; the hydroxyl group of compound **16** interacted with Arg74 on the loop structure connected to the short helix S1; and the methoxy group located on the opposite face of the molecule could establish a hydrogen bond with Leu89 on the loop structure attached to the long helix B, with this fulfilling the firm binding and inhibition of IL-6.

Compound **17** is an epoxy-7-sitosterol, and the epoxy and carbonyl groups appeared to be the key functional elements. In the molecular docking analysis, hydrogen bonds formed by the epoxy group and carbonyl group of compound **17** with the amino acid residues of IL-1β were observed. At the same time, the ergosterol derivatives without these two substituents (compounds **15** and **16**) exhibited no activity against IL-1β; these two substituents of compound **17** also played essential roles in combination with the IκB-α/NF-κB complex, as they could establish hydrogen bonds with the NF-κB-P65 (chain A) and IκB-α (chain D), respectively, to form an IκB-α/NF-κB-P65/inhibitor (compound **17**) complex. This increased the binding affinity of IκB-α and NF-κB-P65, suggesting that the external factor-stimulated phosphorylation and degradation of IκB-α could subsequently be inhibited to certain degrees. The release of NF-κB-P65 from IκB-α; and the following relocation of NF-κB-P65 from the cytoplasm to the nucleus were suppressed, implying that the activation of NF-κB would be prevented [39]. This inference can be supported by the present data from Western blots. Thus, we can conclude that compound **17** exerts an anti-inflammatory effect by affecting the NF-κB signaling pathway. This research was mainly carried out by performing experiments on in vitro cell models and computer simulations. The results cannot fully elucidate the tested compounds' actual effects and mechanisms of action. In vivo studies and clinical trials are needed to confirm these findings.

4. Materials and Methods

4.1. Fungi Material

The mature fruiting bodies of *D. indusiata* were collected from the Yibin edible fungi cultivation base (28°364″ N; 104°867″ E), Sichuan, China. The collection was performed in September 2021. The voucher specimen (No. D.I-B002) was deposited in the Key Laboratory of National Forestry and Grassland Administration/Beijing for Bamboo & Rattan Science and Technology, Beijing, China.

4.2. Chemicals and Reagents

The chromatographically pure reagents were purchased from Fisher-Scientific (Pittsburgh, PA, USA), ultrapure water was obtained using a PALL Lab Water Purification System (Port Washington, NY, USA), and other analytically pure reagents were supplied by Sinopharm (Beijing, China).

Dulbecco's modified Eagle's minimum essential medium (DMEM), fetal bovine serum (FBS), bovine serum albumin (BSA), and penicillin/streptomycin solution were obtained from Life Technologies, Inc. (Grand Island, NY, USA). Lipopolysaccharide (LPS) (*Escherichia coli*, serotype 055:B5), 3-(4,5-dimethylthiazol-2-yl)-2,5-diphenyl tetrazolium bromide (MTT), and dimethyl sulfoxide (DMSO) were obtained from Sigma–Aldrich (St. Louis, MO, USA). Glyceraldehyde-3-phosphate dehydrogenase (GAPDH), primary antibodies against iNOS and *p*-IκB-α were obtained from Cell Signaling Technology (Danvers, MA, USA). The nitric oxide (NO) assay kit (S0021) and the mouse TNF-α, IL-6, and IL-1β ELISA kits (PT512, PI326, and PI301, respectively) were purchased from Beyotime Biochemical (Haimen, China).

4.3. Cell Culture

The mouse microglial cell line BV-2 was obtained from the Institute of Basic Medical Sciences, Chinese Academy of Medical Sciences (Beijing, China). The cells were cultured in DMEM supplemented with 10% FBS and 1% penicillin/streptomycin at 37 °C in a humidified incubator with an atmosphere of 5% CO_2.

4.4. General Experimental Procedures

The isolation of the compounds was performed by using repeated open-column chromatography (CC), preparative thin-layer chromatography (TLC), and preparative high-performance liquid chromatography (HPLC). The chemical structure of the isolated compounds was determined by the spectra of analytical HPLC, UV, ^{1}H and ^{13}C-NMR, HRESIMS, CD, and XRD. Instrumental details were described in Supplementary Materials (Table S1).

4.5. Extraction and Isolation

After air-dried, 50 kg *D. indusiata* fruiting bodies were repeatedly extracted four times with 85% EtOH under reflux. The resulting extracts were combined and filtered (No.1 filter paper Whatman, Maidstone, England), then evaporated under reduced pressure using a rotary evaporator (R-215, Buchi, Flawil, Switzerland) to give an organic solvent-free crude extract: 12.60 kg. The crude extract was resuspended in water and then partitioned with EtOAc. The EtOAc-partitioned extract (800 g) was chromatographed on a silica gel column with gradient elution of CH_2Cl_2/MeOH (200:1, 100:1, 30:1, 10:1, 5:1, 2:1, 0:1, *v/v*) to give 28 fractions (ZS1–ZS28). The fractions with comparatively high yields, including ZS7 (9.7 g), ZS12 (13.2 g), ZS13 (6.3 g), ZS14 (7.6 g), ZS24 (50.6 g), and ZS27 (4.7 g), were subjected to the further separations. Fraction ZS7 was separated into five subfractions ZS7a–ZS7e on a silica gel column eluted with CH_2Cl_2/MeOH (5:1, 2:1, *v/v*) and MeOH. ZS7c (4.4 g) was submitted to a Sephadex LH-20 column, eluted with petroleum ether/CH_2Cl_2/MeOH (5:5:1, *v/v*), followed by a separation on preparative HPLC using eluting solvents of MeCN/H_2O (95:5, *v/v*), MeOH/H_2O (55:45, *v/v*), and MeOH, to obtain compound **13** (23.0 mg), compound **11** (6.1 mg) and compound **14** (1.5 g). Fraction ZS12 was subjected to a Sephadex LH-20 column eluted with a gradient system of petroleum ether/CH_2Cl_2/MeOH (10:10:1

to 1:1:3, *v/v*) and MeOH to yield 11 subfractions (ZS12a–ZS12k). ZS12i was proven to be a single compound **10** (58.00 mg) by HPLC analysis. Fraction ZS13 was separated on a Sephadex LH-20 column eluted with petroleum ether/CH_2Cl_2 (5:1, *v/v*) to yield six subfractions (ZS13a–ZS13f). The separation of ZS13a was conducted on a preparative TLC using petroleum ether/CH_2Cl_2/MeOH (7:7:1, *v/v*) as the elution solvent, followed by a preparative HPLC (MeOH/H_2O, 80:20, *v/v*) to obtain compound **17** (4.8 mg) and compound **18** (2.9 mg). Same preparative thin layer chromatography separations were carried out on ZS13c, ZS13d, ZS13e, and ZS13f, and these four fractions were further separated by preparative HPLC eluted with MeOH/H_2O (70:30, *v/v*), MeOH/H_2O (70:30, *v/v*), MeOH/H_2O (60:40, *v/v*), and MeOH/H_2O (87:13, *v/v*), respectively, to obtain compound **4** (7.9 mg), compound **2** (2.9 mg), compound **1** (1.6 mg), and compound **7** (5 mg). Fraction ZS27 was separated using a Sephadex LH-20 column eluted with petroleum ether/CH_2Cl_2/MeOH (2:2:1, *v/v*) to yield nine subfractions (ZS27a–ZS27i). ZS27f was submitted to preparative TLC eluted with petroleum ether/CH_2Cl_2/MeOH (3:3:1, *v/v*) and further purified on a preparative HPLC (MeOH/H_2O, 20:80, *v/v*) to obtain compound **12** (1.2 mg). ZS27d, ZS27h, and ZS27i were isolated by preparative HPLC with different elution solvents of MeOH/H_2O (55:45, *v/v*), MeOH/H_2O (31:69, *v/v*), and MeOH/H_2O (36:64, *v/v*), to afford compound **5** (1.5 mg), compound **3** (12 mg), and compound **9** (15 mg), respectively. Fraction ZS24 was purified on a silica gel column, eluted with a gradient of CH_2Cl_2/MeOH (6:1 to 0:1, *v/v*), and further isolated by preparative HPLC (MeOH/H_2O, 10:90, *v/v*) to give compound **6** (50 mg). Fraction ZS14 was also chromatographed on a Sephadex LH-20 column eluted with petroleum ether/CH_2Cl_2/MeOH (5:5:1, *v/v*) to yield five subfractions (ZS14a to ZS14e). ZS14b and ZS14d were further separated using a Sephadex LH-20 column eluted with petroleum ether/CH_2Cl_2 (1:1, *v/v*), then subjected to a preparative HPLC eluted with MeOH to obtain compound **15** (3.5 mg), compound **16** (7.7 mg), and compound **8** (2.7 mg).

Characterization data of previously undescribed compounds:

Compound **1**: yellowish amorphous powder, UV(MeOH) λ_{max} 248.7 nm; HRESIMS *m/z*: 235.1690 $[M + H]^+$ (calcd for $C_{15}H_{22}O_2$, 235.1693). [^1]H NMR data (DMSO-d_6, 500 MHz) and [^13]C-NMR data (DMSO-d_6, 125 MHz) are shown in Table 1. CD spectrum (MeOH) is shown in Figure 3.

Crystal data: $C_{15}H_{22}O_2$, M = 234.32, orthorhombic, a = 7.4315(7) Å, b = 13.1582(12) Å, c = 26.367(2) Å, U = 2578.3(4) Å^3, T = 111.6(9), space group $C222_1$ (no. 20), Z = 8, μ(Cu Kα) = 0.612, 4187 reflections measured, 2412 unique (R_{int} = 0.0675) which were used in all calculations. The final $wR(F_2)$ was 0.1293.

Compound **2**: yellowish oil, UV(MeOH) λ_{max} 235.7 nm; HRESIMS *m/z*: 235.1694 $[M + H]^+$ (calcd for $C_{15}H_{22}O_2$, 235.1693). [^1]H NMR data (DMSO-d_6, 500 MHz) and [^13]C-NMR data (DMSO-d_6, 125 MHz) are shown in Table 1. CD spectrum (MeOH) is shown in Figure 3.

Compound **3**: brown crystal, UV(MeOH) λ_{max} 229.8 nm; HRESIMS *m/z*: 306.0981 $[M + H]^-$ (calcd for $C_{15}H_{15}NO_6$, 306.0972). [^1]H NMR data (DMSO-d_6, 500 MHz) and [^13]C-NMR data (DMSO-d_6, 125 MHz) are shown in Table 1. CD spectrum (MeOH) is shown in Figure 3.

Crystal data: $C_{15}H_{15}NO_7$, M = 321.28, trigonal, a = 26.3585(15) Å, c = 5.4846(4) Å, U = 3300.1(4) Å^3, T = 113(2), space group R3 (no. 146), Z = 9, μ(Cu Kα) = 0.998, 5982 reflections measured, 2699 unique (R_{int} = 0.0302), which were used in all calculations. The final $wR(F_2)$ was 0.1274.

Compound **4**: yellowish oil, UV(MeOH) λ_{max} 277.1 nm; HRESIMS *m/z*: 225.1482 $[M + H]^-$ (calcd for $C_{13}H_{20}O_3$, 225.1485). [^1]H NMR data (DMSO-d_6, 500 MHz) and [^13]C-NMR data (DMSO-d_6, 125 MHz) are shown in Table 1. CD spectrum (MeOH) is shown in Figure 3.

4.6. In Vitro Anti-Inflammatory Assay

Compounds **1**, **3**, **4**, **11**, **15**, **16**, and **17** were selected for in vitro investigations of anti-inflammatory activities using an LPS-stimulated BV-2 microglial cell model. Three groups were designed for the experiments: the normal cell group, where the cells were cultured under normal growth conditions; the LPS group, where the cells were treated with LPS but without the tested compounds; and the sample group, where the cells were treated with LPS plus the tested compounds.

4.6.1. MTT Assay for the Measurement of Cell Viability

The cytotoxic effects of the selected compounds on the BV-2 cells were evaluated using an MTT assay [38]. Briefly, BV-2 cells were seeded into 96-well plates at a density of 8×10^3 cells/well and cultured overnight in an incubator at 37 °C with 5% CO_2. Then, the cells were treated with different concentrations of the selected compounds diluted with DMEM. After 2 h, LPS (1 μg/mL) was added. After 24 h of incubation, 20 μM MTT was added to each well and the cells were incubated at 37 °C for 4 h. Afterward, the supernatant was discarded, and 150 μL of DMSO was added to each well to dissolve the formazan. The absorbance (optical density, OD) of each well was measured at 490 nm using a multilabel plate reader (Victor 2030, PerkinElmer, Waltham, MA, USA). The cell viability results were calculated as percentages.

4.6.2. Measurement of Nitric Oxide and Cytokine Production

The tested compounds were diluted in a gradient with DMEM. The BV-2 cells were seeded into 96-well plates at a density of 8×10^3 cells/well, cultured overnight in an incubator at 37 °C with 5% CO_2, and then cultured with LPS (1 μg/mL) in the absence or presence of the tested compounds for 24 h. The culture supernatants were collected for the measurements. The total nitric oxide level was measured using the NO assay kit. The TNF-α, IL-1β, and IL-6 concentrations were quantified using mouse ELISA kits. All operations were conducted according to the manufacturer's instructions.

4.6.3. Western Blot Analysis

The protein expressions of iNOS and p-IκB-α were measured using a Western blot analysis [74]. The tested-compound-treated BV-2 cells in the logarithmic growth phase were digested in a single-cell suspension with trypsin and seeded into 6-well plates at a density of 3×10^5 cells/well. Then, the cells were washed twice with 4 °C phosphate-buffered saline (PBS) and harvested. Next, 200 μL of radioimmunoprecipitation assay (RIPA) buffer was added to each well, and the lysate was centrifuged at $12,000 \times g$ for 20 min after incubation at 4 °C for 30 min. The protein concentration was determined using a bicinchoninic acid (BCA) assay. The protein was collected for Western blot analyses of iNOS and p-IκB-α. After being resolved using SDS/PAGE loading buffer, the protein was electrophoretically separated at 120 V for 90 min and transferred to polyvinylidence difluoride (PVD) membranes at 300 mA for 85 min. Then, the PVD membranes were blocked with 5% skim milk in phosphate-buffered saline containing 0.05% Tween-20 (PBST) for 120 min at room temperature. The cells were incubated overnight at 4 °C in diluted primary antibodies (anti-iNOS and anti-p-IκB-α). The membrane was washed with PBST three times and incubated in a (horseradish peroxidase) HRP-conjugated secondary antibody solution for 120 min at room temperature. Finally, an appropriate amount of enhanced chemiluminescence reagent was added to detect the protein. The data for iNOS and p-IκB-α were normalized on the basis of GAPDH levels.

4.7. Molecular Docking

The protein structures of TNF-α (PDB ID: 7KP8), IL-1β (PDB ID: 8I1B), iNOS (PDB ID: 4UX6), and IL-6 (PDB ID: 2L3Y) were downloaded from the Protein Data Bank (http://www.rcsb.org/, accessed on 1 February 2023). The structure of the IκB-α/NF-κB complex (PDB ID: 1IKN) was modeled using SwissModel (http://swissmodel.expasy.org/, accessed

on 1 February 2023) to remove the repeats of subunits from the heterodimer [42]. Each structure was prepared and refined using the Protein Preparation Wizard of Maestro 11.9 (Schrodinger LLC, New York, NY, USA). Hydrogens were added, water molecules were removed, energy was optimized, and the force-field parameters were adjusted to make them a low-energy conformation satisfying the ligand structure [75]. The amino acids were modified with a flexible setting, and the polar hydrogen atoms of the specific amino acids in the binding pocket were allowed to rotate during the optimization of the docking poses. The 3D structures of compounds **3**, **15**, **16**, and **17** were created and optimized to lower-energy conformers with the Maestro Build Panel, and they were used as the ligands for the molecular docking simulations. The glide ligand docking and induced-fit docking modules in Maestro 11.9 software were employed for the docking study and for the analysis of the results [76,77]. The docking results were visualized using USCF ChimeraX (https://www.rbvi.ucsf.edu/chimerax, accessed on 1 February 2023).

4.8. Statistical Analysis

Each experiment was repeated three times, with three replicates within each experiment. The data are expressed as mean $\pm$ standard deviations (SD). IBM SPSS software (version 23.0, SPSS Inc. Chicago, IL, USA) was used to generate graphs and perform statistical analyses. Data were analyzed using a Student's t-test and one-way analysis of variance (ANOVA). A p-value < 0.05 was considered statistically significant.

5. Conclusions

A chemical investigation of the ethyl acetate fraction of *D. indusiata* ethanolic extract resulted in the isolation and identification of 18 compounds (**1–18**), including three previously undescribed sesquiterpenoids (**1**, **2**, and **4**) and one previously undescribed quinolone derivate (**3**). Their structures and absolute configurations were elucidated using spectroscopic methods and chemical analyses. Among them, compound **1** was the first natural product identified from fungi with an unusual molecular skeleton of antsorane. Seven isolated compounds were evaluated for anti-inflammatory activities in an LPS-stimulated BV-2 microglial cell model. Compound **3** had the best inhibitory effect on TNF-α secretion. Compound **16**, an ergosterol derivative with a rearranged tetracyclic skeleton, showed the most potent activity on the suppression of IL-6 generation. The $5\alpha,6\alpha$-epoxy-7-sitosterol compound **17** exhibited an anti-inflammatory effect by inhibiting the production of NO and IL-1β and the expressions of iNOS and p-IκB-α. The molecular docking study conducted in this research indicated that the tested compounds could exert their anti-inflammatory activities by binding to the hydrophobic pocket of the corresponding protein. These findings suggest that, as *D. indusiata* is an edible and medicinal mushroom, its anti-inflammatory property would be at least partially contributed by the presence of a series of compounds with small molecular weights as active constituents. The results of this study demonstrate the chemodiversity and biological potential of the small-molecule metabolites in *D. indusiata*. They provide a foundation for future investigations into the molecular basis of the pharmacological effects of the mushroom *Dictyophora indusiata*.

Author Contributions: Conceptualization, J.S. and Q.G.; methodology, J.S. and H.X.; software, Y.Z. and F.Q.; validation, H.X. and Q.G.; formal analysis, Y.Z. and J.S.; investigation, Y.Z. and H.X.; resources, F.T.; data curation, J.S.; writing—original draft preparation, Y.Z.; writing—review and editing, H.X.; visualization, Q.G.; supervision, F.T.; project administration, J.S.; funding acquisition, F.T. All authors have read and agreed to the published version of the manuscript.

References

1. Habtemariam, S. The chemistry, pharmacology and therapeutic potential of the edible mushroom *Dictyophora indusiata* (*Vent ex. Pers.*) Fischer (Synn. *Phallus indusiatus*). *Biomedicines* **2019**, *7*, 98. [CrossRef]
2. Wu, Q.; Dai, T.; Song, J.; Liu, X.; Song, S.; Li, L.; Liu, J.; Pugazhendhi, A.; Jacob, J.A. Effects of herbal and mushroom formulations used in traditional Chinese medicine on in vitro human cancer cell lines at the preclinical level: An empirical review of the cell killing mechanisms. *Process Biochem.* **2020**, *94*, 136–142. [CrossRef]
3. Elkhateeb, W.; Daba, G.; Elnahas, M.; Thomas, P. *Trametes versicolor* and *Dictyophora indusiata* champions of medicinal mushrooms. *Pharm. Res.* **2020**, *4*, 00019. [CrossRef]
4. Ker, Y.-B.; Chen, K.-C.; Peng, C.-C.; Hsieh, C.-L.; Peng, R.Y. Structural characteristics and antioxidative capability of the soluble polysaccharides present in *Dictyophora indusiata* (*Vent. Ex Pers.*) Fish *Phallaceae. Evid.-Based Complement. Altern. Med.* **2011**, *2011*, 396013. [CrossRef]
5. Wang, Y.; Shi, X.; Yin, J.; Nie, S. Bioactive polysaccharide from edible *Dictyophora* spp.: Extraction, purification, structural features and bioactivities. *Bioact. Carbohydr. Diet. Fibre* **2018**, *14*, 25–32. [CrossRef]
6. Kawagishi, H.; Ishiyama, D.; Mori, H.; Sakamoto, H.; Ishiguro, Y.; Furukawa, S.; Li, J.X. Dictyophorines A and B, two stimulators of NGF-synthesis from the mushroom *Dictyophora indusiata*. *Phytochem* **1997**, *45*, 1203–1205. [CrossRef] [PubMed]
7. Ishiyama, D.; Fukushi, Y.; Ohnishi-Kameyama, M.; Nagata, T.; Mori, H.; Inakuma, T.; Ishiguro, Y.; Li, J.; Kawagishi, H. Monoterpene-alcohols from a mushroom *Dictyophora indusiata*. *Phytochem* **1999**, *50*, 1053–1056. [CrossRef]
8. Huang, M.; Chen, X.; Tian, H.; Sun, B.; Chen, H. Isolation and identification of antibiotic albaflavenone from *Dictyophora indusiata* (*Vent: Pers.*) Fischer. *J. Chem. Res.* **2011**, *35*, 659–660. [CrossRef]
9. Zhang, Y.-F.; Xun, H.; Gao, Q.; Tang, F.; Qi, F.-F.; Sun, J. Two New Sesquiterpenoids from *Dictyophora indusiata*. *J. Asian Nat. Prod. Res.* **2022**, *24*, 1–7. [CrossRef]
10. Lee, S.R.; Lee, D.; Lee, B.S.; Ryoo, R.; Pang, C.; Kang, K.S.; Kim, K.H. Phallac Acids A and B, New Sesquiterpenes from the Fruiting Bodies of *Phallus luteus*. *J. Antibiot.* **2020**, *73*, 729–732. [CrossRef]
11. Lee, I.-K.; Yun, B.-S.; Han, G.; Cho, D.-H.; Kim, Y.-H.; Yoo, I.-D. Dictyoquinazols, A, B, and C, New neuroprotective compounds from the mushroom *Dictyophora indusiata*. *J. Nat. Prod.* **2002**, *65*, 1769–1772. [CrossRef] [PubMed]
12. Sharma, V.K.; Choi, J.; Sharma, N.; Choi, M.; Seo, S.-Y. In vitro anti-tyrosinase activity of 5-(hydroxymethyl)-2-furfural isolated from *Dictyophora indusiata*. *Phytother. Res.* **2004**, *18*, 841–844. [CrossRef] [PubMed]
13. Okin, D.; Medzhitov, R. Evolution of inflammatory diseases. *Curr. Biol.* **2012**, *22*, R733–R740. [CrossRef] [PubMed]
14. Scheinfeld, N. A comprehensive review and evaluation of the side effects of the tumor necrosis factor alpha blockers etanercept, infliximab and adalimumab. *J. Dermatolog. Treat.* **2004**, *15*, 280–294. [CrossRef] [PubMed]
15. Kumar, K.; Mehra, R.; Guiné, R.P.F.; Lima, M.J.; Kumar, N.; Kaushik, R.; Ahmed, N.; Yadav, A.N.; Kumar, H. Edible Mushrooms: A comprehensive review on bioactive compounds with health benefits and processing aspects. *Foods* **2021**, *10*, 2996. [CrossRef]
16. Venturella, G.; Ferraro, V.; Cirlincione, F.; Gargano, M.L. Medicinal mushrooms: Bioactive compounds, use, and clinical trials. *Int. J. Mol. Sci.* **2021**, *22*, 634. [CrossRef]
17. Ji, W.H.; Kim, J.; Kim, H.; Jang, W.; Kim, K.H. Mushrooms: An important source of natural bioactive compounds. *Nat. Prod. Sci.* **2020**, *26*, 118–131. [CrossRef]
18. Wang, Y.; Ji, X.; Yan, M.; Chen, X.; Kang, M.; Teng, L.; Wu, X.; Chen, J.; Deng, C. Protective effect and mechanism of polysaccharide from *Dictyophora indusiata* on dextran sodium sulfate-induced colitis in C57BL/6 mice. *Int. J. Biol. Macromol.* **2019**, *140*, 973–984. [CrossRef]
19. Kanwal, S.; Joseph, T.P.; Aliya, S.; Song, S.; Saleem, M.Z.; Nisar, M.A.; Wang, Y.; Meyiah, A.; Ma, Y.; Xin, Y. Attenuation of DSS induced colitis by *Dictyophora indusiata* polysaccharide (DIP) via modulation of gut microbiota and inflammatory related signaling pathways. *J. Func. Foods* **2020**, *64*, 103641. [CrossRef]

20. Hara, C.; Kiho, T.; Tanaka, Y.; Ukai, S. Anti-inflammatory activity and conformational behavior of a branched (1→3)-β-d-glucan from an alkaline extract of *Dictyophora indusiata* fisch. *Carbohydr. Res.* **1982**, *110*, 77–87. [CrossRef]

21. Xie, Y.Q.; Du, X.Y.; Liu, D.; Chen, X.Q.; Li, R.T.; Zhang, Z.J. Chemical constituents from *Laggera pterodonta* and their anti-inflammatory activities in vitro. *Phytochem. Lett.* **2021**, *43*, 126–129. [CrossRef]

22. Ablajan, N.; Zhao, B.; Wenjuan, X.; Zhao, J.; Sagdullaev, S.S.; Guoan, Z.; Aisa, H.A. Chemical components of *Aconitum barbatum* var. *puberulum* and their cytotoxic and antibacterial activities. *Nat. Prod. Res.* **2021**, *35*, 1–4. [CrossRef] [PubMed]

23. Ramasamy, D.; Saraswathy, A. Vitiquinolone–a quinolone alkaloid from *Hibiscus vitifolius* Linn. *Food Chem.* **2014**, *145*, 970–975. [CrossRef] [PubMed]

24. Shen, Y.M.; Mu, Q.Z. New Furans from *Cirsium chlorolepis*. *Planta Med.* **1990**, *56*, 472–474. [CrossRef] [PubMed]

25. Wang, Z.W.; Li, Y.; Liu, D.H.; Mu, Y.; Dong, H.J.; Zhou, H.L.; Guo, L.P.; Wang, X. Four new phenolic constituents from the rhizomes of *Gastrodia elata* Blume. *Nat. Prod. Res.* **2019**, *33*, 1140–1146. [CrossRef] [PubMed]

26. Bering, L.; Craven, E.J.; Sowerby Thomas, S.A.; Shepherd, S.A.; Micklefield, J. Merging enzymes with chemocatalysis for amide bond synthesis. *Nat. Commun.* **2022**, *13*, 380. [CrossRef]

27. Guo, Y.; Li, X.; Wang, J.; Xu, J.; Li, N. A new alkaloid from the fruits of *Celastrus orbiculatus*. *Fitoterapia* **2005**, *76*, 273–275. [CrossRef]

28. Weng, I.T.; Lin, Y.A.; Chen, G.Y.; Chiang, H.M.; Liu, Y.J.; Chen, C.J.; Lan, Y.H.; Lee, C.L. (-)-β-Homoarginine anhydride, a new antioxidant and tyrosinase inhibitor, and further active components from *Trichosanthes truncata*. *Nat. Prod. Res.* **2020**, *34*, 2262–2268. [CrossRef]

29. Sadhu, S.K.; Phattanawasin, P.; Choudhuri, M.S.K.; Ohtsuki, T.; Ishibashi, M. A new lignan from *Aphanamixis polystachya*. *J. Nat. Med.* **2006**, *60*, 258–260. [CrossRef]

30. Abdelrheem, D.A.; Rahman, A.A.; Elsayed, K.N.M.; Abd El-Mageed, H.R.; Mohamed, H.S.; Ahmed, S.A. Isolation, characterization, *in vitro* anticancer activity, dft calculations, molecular docking, bioactivity score, drug-likeness and admet studies of eight phytoconstituents from brown alga *sargassum platycarpum*. *J. Mol. Struct.* **2021**, *1225*, 129245. [CrossRef]

31. Nakada, T.; Yamamura, S. Three New Metabolites of Hybrid Strain KO 0231, Derived from Penicillium *citreo-viride* IFO 6200 and 4692. *Tetrahedron* **2000**, *56*, 2595–2602. [CrossRef]

32. Aiello, A.; Fattorusso, E.; Magno, S.; Mayol, L.; Menna, M. Isolation of two novel 5α,6α-Epoxy-7-ketosterols from the Encrusting Demospongia Oscarella lobularis. *J. Nat. Prod.* **1990**, *53*, 487–491. [CrossRef]

33. Lee, D.; Lee, S.R.; Kang, K.S.; Kim, K.H. Bioactive Phytochemicals from Mulberry: Potential anti-inflammatory effects in lipopolysaccharide-stimulated RAW 264.7 macrophages. *Int. J. Mol. Sci.* **2021**, *2*, 8120. [CrossRef] [PubMed]

34. Muszyńska, B.; Grzywacz-Kisielewska, A.; Kała, K.; Gdula-Argasińska, J. Anti-inflammatory properties of edible mushrooms: A review. *Food Chem.* **2018**, *243*, 373–381. [CrossRef] [PubMed]

35. Deshmukh, S.K.; Verekar, S.A.; Periyasamy, G.; Ganguli, B.N. Fungi: A Potential Source of Anti-inflamatory Compounds. In *Microorganisms in Sustainable Agriculture and Biotechnology*; Johri, B.N., Prakash, A., Eds.; Springer: Dordrecht, The Netherlands, 2016; pp. 613–645. [CrossRef]

36. Tolosa, L.; Donato, M.T.; Gómez-Lechón, M.J. General cytotoxicity assessment by means of the MTT assay. *Methods Mol. Biol.* **2015**, *1250*, 333–348. [CrossRef]

37. Colasanti, M.; Persichini, T.; Menegazzi, M.; Mariotto, S.; Giordano, E.; Caldarera, C.M.; Sogos, V.; Lauro, G.M.; Suzuki, H. Induction of nitric oxide synthase mRNA expression: Suppression by exogenous nitric oxide. *J. Biol. Chem.* **1995**, *270*, 26731–26733. [CrossRef]

38. Sun, J.; Zhang, X.; Broderick, M.; Fein, H. Measurement of nitric oxide production in biological systems by using Griess reaction assay. *Sensors* **2003**, *3*, 276–284. [CrossRef]

39. Lee, J.-I.; Burckart, G.J. Nuclear Factor Kappa B: Important transcription factor and therapeutic target. *J. Clin. Pharmacol.* **1998**, *38*, 981–993. [CrossRef]

40. Cheshire, D.R.; Åberg, A.; Andersson, G.M.K.; Andrews, G.; Beaton, H.G.; Birkinshaw, T.N.; Boughton-Smith, N.; Connolly, S.; Cook, T.R.; Cooper, A.; et al. The discovery of novel, potent and highly selective inhibitors of inducible nitric oxide synthase (iNOS). *Bioorg. Med. Chem. Lett.* **2011**, *21*, 2468–2471. [CrossRef]

41. He, M.M.; Smith, A.S.; Oslob, J.D.; Flanagan, W.M.; Braisted, A.C.; Whitty, A.; Cancilla, M.T.; Wang, J.; Lugovskoy, A.A.; Yoburn, J.C.; et al. Small-Molecule Inhibition of TNF-α. *Science* **2005**, *310*, 1022–1025. [CrossRef]

42. Huxford, T.; Huang, D.-B.; Malek, S.; Ghosh, G. The Crystal Structure of the IκBα/NF-κB Complex Reveals Mechanisms of NF-κB Inactivation. *Cell* **1998**, *95*, 759–770. [CrossRef]

43. Wang, J.; Wen, X.; Zhang, Y.; Zou, P.; Cheng, L.; Gan, R.; Li, X.; Liu, D.; Geng, F. Quantitative proteomic and metabolomic analysis of *Dictyophora indusiata* fruiting bodies during post-harvest morphological development. *Food Chem.* **2021**, *339*, 127884. [CrossRef]

44. Chen, H.-Y.; Lei, J.-Y.; Li, S.-L.; Guo, L.-Q.; Lin, J.-F.; Wu, G.-H.; Lu, J.; Ye, Z.-W. Progress in biological activities and biosynthesis of edible fungi terpenoids. *Crit. Rev. Food Sci. Nutr.* **2022**, *62*, 1–23. [CrossRef] [PubMed]

45. Avalos, M.; Garbeva, P.; Vader, L.; van Wezel, G.P.; Dickschat, J.S.; Ulanova, D. Biosynthesis, evolution and ecology of microbial terpenoids. *Nat. Prod. Rep.* **2022**, *39*, 249–272. [CrossRef] [PubMed]

46. Chazan, J.B. L'Antsorenone, cétone sesquiterpénique de l'huile essentielle *d'Elionurus tristis*. In *Rapport d'activité, Tananarive*; Institut Français de Recherche Scientifique pour le Développement en Coopération (ORSTOM): Montpellier, France, 1969; pp. 29–31.

47. Garcia, G.P.; Sutour, S.; Rabehaja, D.; Tissandié, L.; Filippi, J.-J.; Tomi, F. Essential oil of the malagasy grass *Elionurus tristis* Hack. contains several undescribed sesquiterpenoids. *Phytochem* **2019**, *162*, 29–38. [CrossRef] [PubMed]

48. Hu, C.-L.; Xiong, J.; Li, J.-Y.; Gao, L.-X.; Wang, W.-X.; Cheng, K.-J.; Yang, G.-X.; Li, J.; Hu, J.-F. Rare sesquiterpenoids from the shed trunk barks of the critically endangered plant *Abies beshanzuensis* and their bioactivities. *Eur. J. Org. Chem.* **2016**, *2016*, 1832–1835. [CrossRef]

49. Rueda, A.; Zubía, E.; Ortega, M.J.; Salvá, J. New Acyclic Sesquiterpenes and Norsesquiterpenes from the Caribbean Gorgonian *Plexaurella grisea*. *J. Nat. Prod.* **2001**, *64*, 401–405. [CrossRef] [PubMed]

50. Xue, S.; Zhang, P.; Tang, P.; Wang, C.; Kong, L.; Luo, J. Acyclic Diterpene and Norsesquiterpene from the Seed of *Aphanamixis polystachya*. *Fitoterapia* **2020**, *142*, 104518. [CrossRef]

51. Carroll, P.J.; Engelhardt, L.M.; Ghisalberti, L.; Jefferies, P.R.; Middleton, E.J.; Mori, T.A.; White, A.H. The Chemistry of *Eremophila* spp. XXII. New Eremane Diterpenes from *E. Fraseri*. *Aust. J. Chem.* **1985**, *38*, 1351. [CrossRef]

52. Champagnat, P.; Bessière, J.-M.; Chezal, J.-M.; Chalchat, J.-C.; Carnat, A.-P. New Compounds from the Essential Oil of *Vetiveria nigritana* Roots from Mali. *Flavour Fragr. J.* **2007**, *22*, 488–493. [CrossRef]

53. Filippi, J.-J. Norsesquiterpenes as Markers of Overheating in Indonesian Vetiver Oil: Norsesquiterpenes of Indonesian Vetiver Oil. *Flavour Fragr. J.* **2014**, *29*, 137–142. [CrossRef]

54. McAfee, B.J.; Taylor, A. A review of the volatile metabolites of fungi found on wood substrates. *Nat. Toxins* **1999**, *7*, 283–303. [CrossRef] [PubMed]

55. Keller, N.P.; Turner, G.; Bennett, J.W. Fungal Secondary Metabolism—From Biochemistry to Genomics. *Nat. Rev. Microbiol.* **2005**, *3*, 937–947. [CrossRef] [PubMed]

56. Zhong, J.-J.; Xiao, J.-H. Secondary Metabolites from Higher Fungi: Discovery, Bioactivity, and Bioproduction. *Adv. Biochem. Eng. Biotechnol.* **2009**, *113*, 79–150. [CrossRef] [PubMed]

57. Bills, G.F.; Gloer, J.B. Biologically Active Secondary Metabolites from the Fungi. *Microbiol. Spectr.* **2016**, *4*, 1087–1119. [CrossRef]

58. Schüffler, A. Secondary Metabolites of Basidiomycetes. In *Physiology and Genetics*, 2nd ed.; Anke, T., Schüffler, A., Eds.; Springer International Publishing: Cham, Switzerland, 2018; pp. 231–275. [CrossRef]

59. Wang, Q.; Cao, R.; Zhang, Y.; Qi, P.; Wang, L.; Fang, S. Biosynthesis and Regulation of Terpenoids from Basidiomycetes: Exploration of New Research. *AMB Express* **2021**, *11*, 150. [CrossRef]

60. Baby, S.; Johnson, A.J.; Govindan, B. Secondary Metabolites from *Ganoderma*. *Phytochemistry* **2015**, *114*, 66–101. [CrossRef]

61. Ahmad, M.F. *Ganoderma Lucidum*: Persuasive Biologically Active Constituents and Their Health Endorsement. *Biomed. Pharmacother.* **2018**, *107*, 507–519. [CrossRef]

62. Cör, D.; Knez, Ž.; Knez Hrnčič, M. Antitumour, Antimicrobial, Antioxidant and Antiacetylcholinesterase Effect of *Ganoderma lucidum* Terpenoids and Polysaccharides: A Review. *Molecules* **2018**, *23*, 649. [CrossRef]

63. Ríos, J.-L. Chemical Constituents and Pharmacological Properties of *Poria Cocos*. *Planta Med.* **2011**, *77*, 681–691. [CrossRef]

64. Lu, J.; Tian, J.; Zhou, L.; Meng, L.; Chen, S.; Ma, C.; Wang, J.; Liu, Z.; Li, C.; Kang, W. Phytochemistry and Biological Activities of *Poria*. *J. Chem.* **2021**, *2021*, 6659775. [CrossRef]

65. Weete, J.D. Structure and function of sterols in fungi. *Adv. Lipid Res.* **1989**, *23*, 115–167. [CrossRef]

66. Zhabinskii, V.N.; Drasar, P.; Khripach, V.A. Structure and biological activity of ergostane-type steroids from fungi. *Molecules* **2022**, *27*, 2103. [CrossRef] [PubMed]

67. Weete, J.D.; Gandhi, S.R. Biochemistry and molecular biology of fungal sterols. In *Biochemistry and Molecular Biology*; Robert, B., George, A.M., Eds.; Springer: Berlin/Heidelberg, Germany, 1996; pp. 421–438. [CrossRef]

68. Phillips, K.M.; Ruggio, D.M.; Horst, R.L.; Minor, B.; Simon, R.R.; Feeney, M.J.; Byrdwell, W.C.; Haytowitz, D.B. Vitamin D and Sterol Composition of 10 types of mushrooms from retail suppliers in the United States. *J. Agric. Food Chem.* **2011**, *59*, 7841–7853. [CrossRef]

69. Shaikh, S.; Verma, H.; Yadav, N.; Jauhari, M.; Bullangowda, J. Applications of steroid in clinical practice: A Review. *ISRN Anesthesiol.* **2012**, *2012*, 985495. [CrossRef]

70. Greuter, T.; Alexander, J.A.; Straumann, A.; Katzka, D.A. Diagnostic and therapeutic long-term management of eosinophilic esophagitis- current concepts and perspectives for steroid use. *Clin. Transl. Gastroenterol.* **2018**, *9*, e212. [CrossRef]

71. Fan, H.; Morand, E.F. Targeting the side effects of steroid therapy in autoimmune diseases: The role of GILZ. *Discov. Med.* **2012**, *13*, 123–133.

72. Duecker, F.L.; Reuß, F.; Heretsch, P. Rearranged ergostane-type natural products: Chemistry, biology, and medicinal aspects. *Org. Biomol. Chem.* **2019**, *17*, 1624–1633. [CrossRef]

73. Veverka, V.; Baker, T.; Redpath, N.T.; Carrington, B.; Muskett, F.W.; Taylor, R.J.; Lawson, A.D.G.; Henry, A.J.; Carr, M.D. Conservation of functional sites on Interleukin-6 and implications for evolution of dignaling complex assembly and therapeutic intervention. *J. Biol. Chem.* **2012**, *287*, 40043–40050. [CrossRef]

74. Kurien, B.T.; Scofield, R.H. Western blotting. *Methods* **2006**, *38*, 283–293. [CrossRef]

75. Madhavi Sastry, G.; Adzhigirey, M.; Day, T.; Annabhimoju, R.; Sherman, W. Protein and ligand preparation: Parameters, protocols, and influence on virtual screening enrichments. *J. Comput. Aided Mol. Des.* **2013**, *27*, 221–234. [CrossRef] [PubMed]

76. Friesner, R.A.; Banks, J.L.; Murphy, R.B.; Halgren, T.A.; Klicic, J.J.; Mainz, D.T.; Repasky, M.P.; Knoll, E.H.; Shelley, M.; Perry, J.K.; et al. Glide: A new approach for rapid, accurate docking and scoring. 1. Method and Assessment of Docking Accuracy. *J. Med. Chem.* **2004**, *47*, 1739–1749. [CrossRef] [PubMed]

77. Sherman, W.; Day, T.; Jacobson, M.P.; Friesner, R.A.; Farid, R. Novel procedure for modeling ligand/receptor induced fit effects. *J. Med. Chem.* **2006**, *49*, 534–553. [CrossRef] [PubMed]